JACS
JOURNAL OF THE AMERICAN CHEMICAL SOCIETY
Article
Cite This: J. Am. Chem. Soc. 2019, 141, 6706−6718
pubs.acs.org/JACS

Mechanism of Action of Peptides That Cause the pH-Triggered Macromolecular Poration of Lipid Bilayers

Sarah Y. Kim,[†] Anna E. Pittman,[‡] Elmer Zapata-Mercado,[†] Gavin M. King,*[,‡,§] William C. Wimley,*[,∥] and Kalina Hristova*[,†]

[†]Department of Materials Science and Engineering, Institute for NanoBioTechnology, and Program in Molecular Biophysics, Johns Hopkins University, Baltimore, Maryland 21218, United States

[‡]Department Physics and Astronomy and [§]Department of Biochemistry, University of Missouri, Columbia, Missouri 65211, United States

[∥]Department of Biochemistry and Molecular Biology, Tulane University School of Medicine, New Orleans, Louisiana 70112, United States

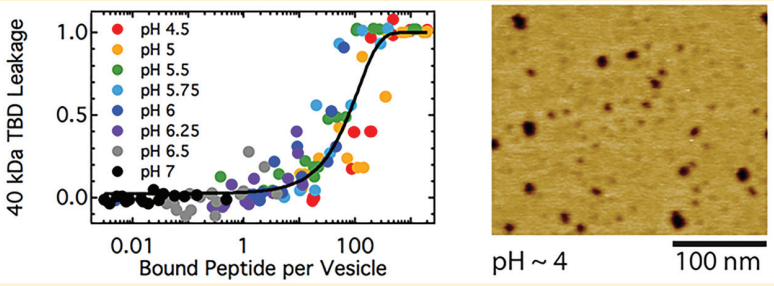

ABSTRACT: Using synthetic molecular evolution, we previously discovered a family of peptides that cause macromolecular poration in synthetic membranes at low peptide concentration in a way that is triggered by acidic pH. To understand the mechanism of action of these "pHD peptides", here we systematically explored structure−function relationships through measurements of the effect of pH and peptide concentration on membrane binding, peptide structure, and the formation of macromolecular-sized pores in membranes. Both AFM and functional assays demonstrate the peptide-induced appearance of large pores in bilayers. Pore formation has a very steep pH dependence and is also dependent on peptide concentration. In vesicles, 50% leakage of 40 kDa dextrans occurs at 1 bound peptide per 1300 lipids or only 75 peptides per vesicle, an observation that holds true across a wide range of acidic pH values. The major role of pH is to regulate the amount of peptide bound per vesicle. The physical chemistry and sequence of the pHD peptides affect their potency and pH dependence; therefore, the sequence−structure−function relationships described here can be used for the future design and optimization of membrane permeabilizing peptides for specific applications.

INTRODUCTION

Membrane-active, pH-sensitive peptides can be utilized for delivering cargo to cells through endosomes[1−3] or for new therapies that target cancer cells,[4−6] among other applications. Although the mechanism of action of several such pH-sensitive peptides has been studied, the peptides previously investigated either insert as monomers without pore formation (i.e., pHLIP) or form only small pores in membranes (e.g., GALA).[7,8] Large pores are needed for most applications. The mechanism of action of pH-sensitive peptides that form large, macromolecule-sized pores will likely involve additional factors such as cooperativity and peptide−peptide interactions. By rationally designing an iterative peptide library based on a pH-insensitive pore-forming peptide, MelP5,[9,10] and using a high-throughput functional screen, we have previously discovered a family of peptides that cause macromolecular poration in synthetic membranes at low concentration in a way that is triggered by acidic pH.[11] These peptides, which we named the pH-dependent delivery (pHD) peptides, are unprecedented in their ability to cause the highly efficient, pH-triggered leakage of large molecules through synthetic membranes. At pH 7 or above, the members of this synthetically evolved family of sequences are essentially inactive; they induce little release of small or large molecules from lipid bilayer vesicles. However, at pH ≤6 they bind to membranes, fold into α-helices, and enable the efficient release of macromolecules at very low peptide concentration.

To understand the mechanism of action of the pHD peptides, here we asked how peptide density on membrane surfaces and cooperativity between peptides promote macromolecule-sized pore formation. Furthermore, we asked how pH regulates these processes. To answer these questions, we examined the structure of the pores formed, and we

Received: February 20, 2019
Published: March 27, 2019

DOI: 10.1021/jacs.9b01970
J. Am. Chem. Soc. 2019, 141, 6706−6718

systematically explored structure–function relationships through measurements of the effect of pH and peptide concentration on membrane binding, peptide structure, and the formation of large pores by the pHD peptides in fluid-phase phosphatidylcholine (PC) membranes.

MATERIALS AND METHODS

Peptides of >95% purity were purchased from BioSynthesis, Inc. 1-Palmitoyl-2-oleoyl-glycero-3-phosphocholine (POPC) and 1-palmitoyl-2-(9,10-dibromo)stearoyl-*sn*-glycero-3-phosphocholine (diBrPSPC) was purchased from Avanti Polar Lipids. 8-Aminonaphthalene-1,2,3-trisulfonic acid (ANTS) and *p*-xylylenebis(pyridinium bromide) (DPX) were purchased from Thermo Fisher Scientific. Chloroform, ammonium thiocyanate, and other salts and buffer materials were purchased from Fisher Scientific or Sigma-Aldrich. TAMRA-biotin-dextran (TBD) was synthesized as described elsewhere.[9,11]

Buffers. Thirteen buffers were prepared with pH from 4 to 7 in 0.25 pH increments. Buffers with a pH of between 4 and 5.5 were prepared with 10 mM sodium acetate, and buffers with a pH of between 5.75 and 7 were prepared with 10 mM sodium phosphate. Buffers for binding and leakage assays were prepared with 100 mM KCl. Buffers for circular dichroism were prepared without KCl, and their pH was adjusted with phosphatidic acid instead of hydrochloric acid to minimize the CD signal due to the absorption of the chloride ion below 200 nm. All buffers were vacuum filtered through a 0.22 μm pore size membrane to remove dust and bacteria before use.

Peptides. Solutions of ∼1 mM peptides were prepared with Millipore water. Concentrations were determined using the absorbance of the single tryptophan on each peptide. The average of three absorbance measurements at 280 nm on a NanoDrop 2000c (Thermo Fisher Scientific) was used to determine the concentration. Peptides were stored frozen until use and were subjected to no more than five freeze–thaws to minimize peptide degradation.

Vesicle Preparation. Three types of 100 nm large unilamellar vesicles (LUV) were prepared with synthetic POPC lipids. For all vesicle types, POPC in chloroform was dried under vacuum overnight, resuspended in buffer, frozen and thawed 5 times, and extruded 10 times through 100 nm polycarbonate membranes. POPC vesicles with no probes entrapped were used for binding and circular dichroism. For TBD-encapsulating vesicles, dry lipid films were resuspended in buffer containing 1 mg of TBD per 50 μmol of lipid. After extrusion, vesicles were incubated on high-capacity streptavidin agarose to remove unencapsulated TBD. For ANTS/DPX vesicles, dried lipid films were resuspended in 12.5 mM ANTS and 45 mM DPX. After extrusion, unencapsulated ANTS and DPX were separated from the vesicles by size exclusion chromatography with Sephadex G-100 resin. The lipid concentration was measured using a modified Stewart assay.[12]

Dextran Leakage Assays. Leakage of 40 kDa was measured with FRET. Dextran vesicles with entrapped TBD were diluted to 1 mM, and streptavidin-AF488 (the donor fluorophore) was added to a final concentration of 20 nM. In a 96-well plate, peptide and vesicles were mixed and then incubated while shaking at room temperature for 1 h before measuring FRET by donor fluorescence quenching on a BioTek H4 Synergy Hybrid Microplate Reader with ex/em = 495/519 nm. As a positive control for 100% leakage, 4 μL of 10% Triton X100 was added to three wells, and as a negative control, no peptide was added to three wells. Leakage measurements are the average of at least three unique vesicle preparations. Fractional leakage was calculated as

$$f_{\text{leakage}} = (F_{\text{no peptide}} - F_{\text{sample}})/(F_{\text{no peptide}} - F_{\text{triton}}) \quad (1)$$

The leakage as a function of pH was fit to determine the pH at which leakage is 50% (the midpoint or "pH50"):

$$f_{\text{leakage}} = L_{\text{max}} + \frac{L_{\text{min}} - L_{\text{max}}}{1 + e^{\text{pH50}-\text{pH}/\text{rate}}} \quad (2)$$

Here, L_{max} and L_{min} are the curve's maximum and minimum values, respectively, and *rate* describes the steepness of the curve.

ANTS/DPX Leakage Assays. Small-molecule leakage was measured by quenching ANTS with DPX. ANTS/DPX leakage vesicles were diluted to 1 mM. On a 96-well plate, peptide and vesicles were mixed at P:L ranging from 1:50 to 1:5000 and then incubated with shaking at room temperature for 1 h before measuring ANTS fluorescence using a microplate reader with ex/em = 360/519 nm. As a positive control for 100% leakage, 4 μL of 10% Triton X100 was added to three wells, and as a negative control, no peptide or Triton was added to three wells. Leakage measurements are the average of at least three unique vesicle preparations. Fractional leakage was calculated as

$$f_{\text{ANTS/DPX leakage}} = (F_{\text{sample}} - F_{\text{no peptide}})/(F_{\text{triton}} - F_{\text{no peptide}}) \quad (3)$$

The leakage as a function of pH was fit using eq 2 to determine the midpoint of the curve, or pH50.

Tryptophan Binding. POPC vesicles were prepared at ∼30 mM at pH 4.75 and pH 6.25 as described above. Vesicles were diluted to 1 mM with buffers spanning pH 4 to 7 and then incubated overnight at 4 °C to allow the internal and external pH to equilibrate while minimizing vesicle degradation due to hydrolysis. The next morning, the pH of the solution was verified with MColorpHast pH test strips. Peptide was added with P:L ranging from 1:50 to 1:5000 in 0.5 mL vials. After 1 h of incubation at room temperature, tryptophan fluorescence spectra were measured on a Horiba Fluorolog 3-22 in a 45 μL cuvette. Samples to correct for lipid scattering, including vesicles, vesicles with tryptophan (at P:L ranging from 1:50 to 1:5000), and tryptophan (at P:L ranging from 1:50 to 1:5000), were also measured at each pH, but without a 1 h incubation. A scattering correction was made as described in ref 13. The midpoint of the curve, or pH50, was obtained by fitting using eq 2.

Circular Dichroism. POPC vesicles without KCl were prepared as described above for the tryptophan binding. Scans were collected in a 1 mm path length cuvette on a JASCO J-710 spectropolarimeter at a scan rate of 100 nm/min, with three accumulations, at room temperature. After measurement, the scans were corrected for background using a vesicle sample with no peptides. The relative % helicity was calculated by scaling the average ellipticity at 222 nm. The midpoint of the curve, or pH50, was obtained by fitting using eq 2.

Tryptophan Quenching. To determine if the pHD peptides can exchange from vesicles to which they are bound into a second population of vesicles added after binding, we measured the change in tryptophan fluorescence upon the addition of a second population of vesicles composed of brominated lipids. Because bromines quench tryptophan fluorescence,[14] the exchange of peptides from POPC to brominated vesicles will result in quenching. We prepared vesicles composed of POPC or 16:0–18:0 (9,10 diBr) PC at pH 4.5 and diluted them to 1 mM. To determine the extent of tryptophan quenching by the brominated vesicles, 100 μL of 1 mM diBrPSPC was mixed with peptide added to a final concentration of 20 μM (P:L = 1:50). After 1 h, the tryptophan fluorescence spectra were measured as described in the binding assay. To measure the kinetics of quenching, the tryptophan fluorescence of pHD15 was measured at 280/334 nm. After adding 100 μL of 1 mM POPC to a cuvette, fluorescence was measured for up to 5 min, and then peptide was added up to a final concentration of 20 μM. After waiting 30 min to ensure maximal binding to the vesicles, diBrPSPC or POPC (as a negative control) was added to a final concentration of 0.2 or 0.33 mM, and fluorescence was measured for 30 more minutes.

Sample Preparation for Atomic Force Microscopy (AFM) Imaging. We adopted established methods to form supported lipid bilayers on mica surfaces.[15] Briefly, POPC was suspended in 300 mM NaCl, 40 mM $CaCl_2$, and 20 mM HEPES, pH 4, at a concentration of 600 μM. Liposomes were prepared by the extrusion of POPC through a polycarbonate membrane with a 100 nm pore diameter. The peptide was diluted to a concentration of 10 μM in imaging buffer: 200 mM NaCl and 50 mM HEPES at pH 4. POPC liposomes were incubated

DOI: 10.1021/jacs.9b01970
J. Am. Chem. Soc. 2019, 141, 6706–6718

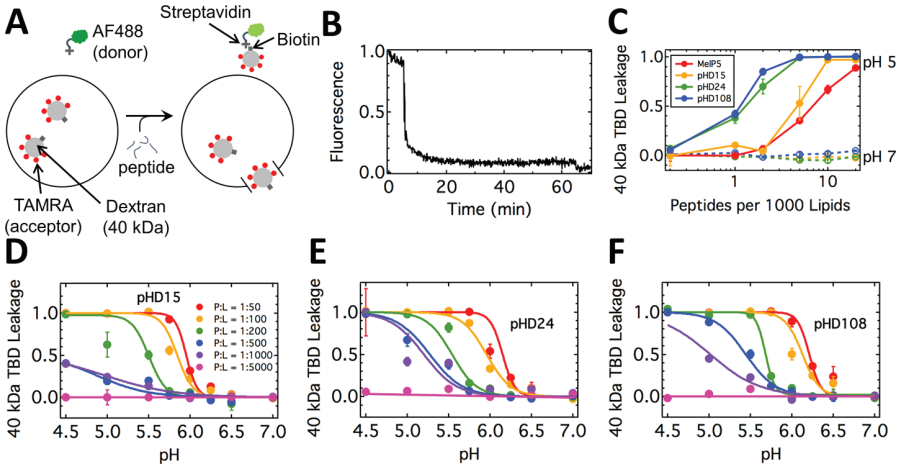

Figure 1. Macromolecular leakage assay. (A) Schematic of the assay. Peptides were incubated with streptavidin-AlexaFluor488 and POPC vesicles containing TAMRA-biotin-dextran (TBD) for 1 h. Upon peptide-mediated macromolecular poration, the 40 kDa dextran can leak out of the vesicles and form a complex with streptavidin, leading to FRET. (B) Time course of streptavidin-AlexaFluor488 (donor) intensity upon TBD vesicle permeabilization. At about t = 5 min, pHD108 (P:L = 1:100) was added to a solution of 1 mM POPC at pH 6. After 1 h, Triton X100 was added for the 100% leakage fluorescence value. (C) Extent of dextran leakage as a function of concentration at pH 5 and 7. At pH 5, the pHD peptides are more potent than MelP5. At pH 7, the pHD peptides are not active, even at the highest concentrations measured. (D–F) Dextran leakage as a function of pH and P:L for pHD15 (D), pHD24 (E), and pHD108 (F).

for 10 min in solution with the peptide to yield a final peptide concentration of 3 μM. The liposomes containing peptides were then deposited onto freshly cleaved mica. Supported bilayers were formed by vesicle fusion (30 min incubation, ~30 °C). Samples were rinsed four times using 75 μL of imaging buffer. Because of rinsing and other factors, P:L assignment during AFM imaging is challenging; we estimate a P:L of roughly 1:100 for all data shown here. For experiments at pH >4, a mixture of 200 mM NaCl and 50 mM Hepes at pH 7 was added to the supported lipid bilayer, resulting in a final pH of approximately 6. All AFM data were collected at ~32 °C, which is significantly above the gel-to-fluid transition temperature of POPC.

AFM Imaging and Analysis. Images were acquired in tapping mode in aqueous buffer solution using a commercial apparatus (Asylum Research Inc., Cypher) and Biolever mini tips with a spring constant of $k \approx 0.9$ N/m (Olympus, BL-AC40TS). Care was taken to control the magnitude of the tip–sample force to ≤100 pN (estimated by comparing the free amplitude to the set-point amplitude). As is typical, images were flattened (second order) to minimize background. For statistical analysis, the data were offset so as to align the population having the greatest height, corresponding to the top surface in each image, to zero. For depth measurements, we assumed that the top surface represented the unmodified surface of the upper leaflet of the supported bilayer; however, is difficult to rule out the formal possibility that this top surface is itself modified by the presence of pHD108 peptides. Individual porelike features were delineated using custom software which uses the Hessian blob strength to identify features from the background, and the footprint area of each feature was reported.[16] The depth of the features was determined using software (Igor Pro, WaveMetrics). Smoothed histograms (kernel density estimates, generated in Igor Pro) were normalized to unity when the abscissa (and ordinate, for the two-dimensional case) was expressed in mks units. Data were fit with Gaussians (MagicPlot), with x_0 defined as the center of the peak.

RESULTS

Peptides Selected for Study. Here, we selected three pHD peptides for detailed characterization. Peptides pHD24 (GIGDVLHELAADLPELQEWIHAAQQL) and pHD108 (GIGEVLHELAEGLPELQEWIHAAQQL) were selected because they are canonical sequences, with five acidic residues like most of the active sequences identified. These two peptides had similarly potent activity and similar pH50 values in our preliminary studies.[11] pHD24 has three aspartate residues and two glutamates, a common acidic residue found across the family, and pHD108 has five glutamates. Peptide pHD15 (GIGEVLHELADDLPDLQEWIHAAQQL) is an outlier which has six acidic residues. Its potency is somewhat lower, and it becomes active at a somewhat lower pH than for the others. We include it here to enable characterization across a range of potencies and pH dependences.

Macromolecular Poration by the pHD Peptides. Using the same fluorescence-based assay we developed for the screen in which we discovered the pHD peptides,[11] we characterized the ability of pHD15, pHD24, and pHD108 to form large pores in vesicles as a function of both pH and peptide concentration. Results from these assays are shown in Figure 1. Figure 1A shows a schematic of the assay. The entrapped probe used to detect macromolecule leakage was a 40 000 Da dextran labeled with the TAMRA dye (fluorescence acceptor) and with biotin (called TBD for TAMRA-biotin-dextran). The external solution contained streptavidin labeled with Alexafluor488 (fluorescence donor). In this assay, the leakage of encapsulated TBD leads to streptavidin–TBD complex formation and the quenching of Alexafluor488 due to FRET.[9,10] The hydrodynamic radius of dextran is about 4.5 nm;[17] therefore, a pore with a radius of at least 45 Å is required to form in the bilayer for dextran leakage to occur. In Figure 1B, we show the kinetics of TBD leakage. Upon addition of peptide to a solution of vesicles at pH 5, the donor fluorescence drops steeply and reaches a plateau. Leakage is rapid, with greater than 90% leakage occurring over 10 min. In Figure 1C, we show the fractional leakage of TBD, measured at 60 min, as a function of the peptide-to-lipid ratio (P:L) at pH 5. pHD24 and pHD108 are very potent at pH 5, with substantial activity observed at concentrations of as low as 1 peptide per 1000 lipids and ≥95% activity at P:L = 1:200. pHD15 is less active, with ≥95% activity occurring at about P:L = 1:100. MelP5, the parent peptide used for library design, is less active than pHD15 with ≥95% activity at P:L > 1:50. No leakage is observed at pH 7 for any of the pHD peptides, even

DOI: 10.1021/jacs.9b01970
J. Am. Chem. Soc. 2019, 141, 6706–6718

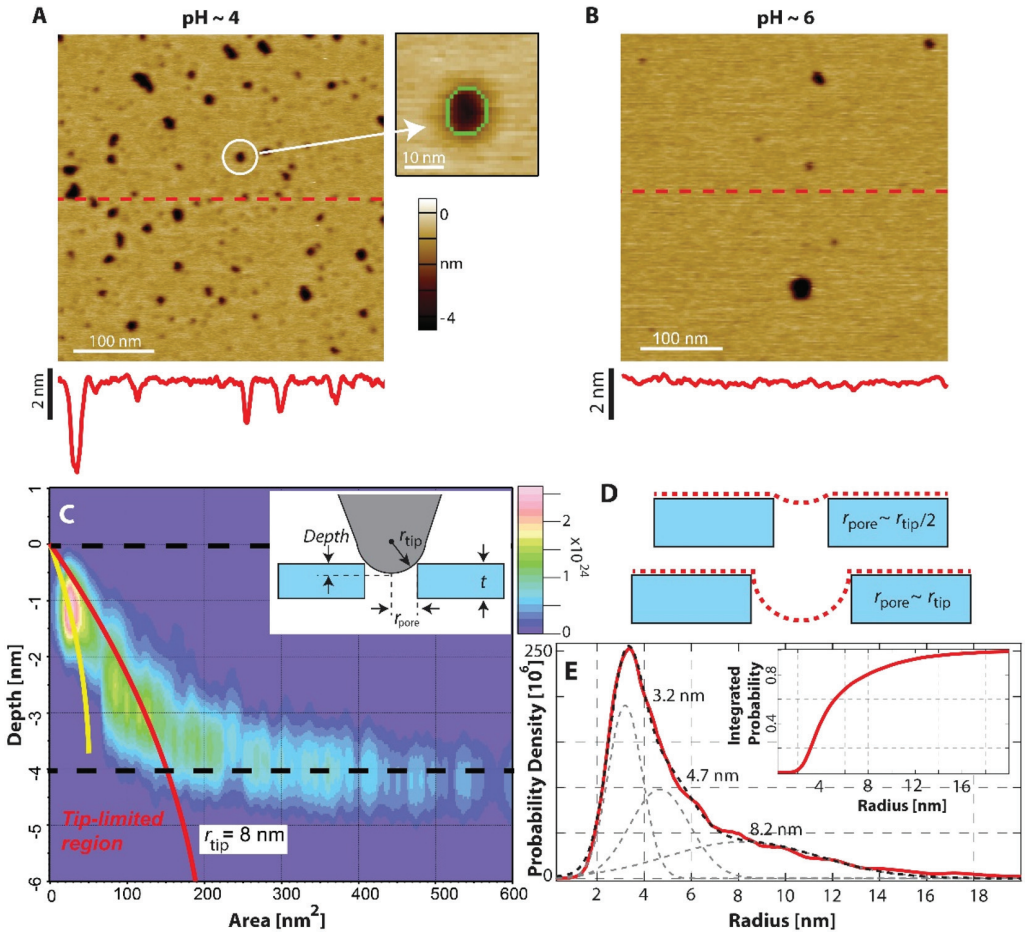

Figure 2. Membrane topography via atomic force microscopy. (A) AFM image at pH 4 showing a variety of punctate porelike features in a POPC bilayer incubated with pHD108. A line scan is shown below the image, with the position indicated by the red dashed line. A detailed view of the feature circled in white shows the result of the Hessian blob algorithm (green perimeter). The area defined by this perimeter was used to compute the effective radius. (B) Image at pH 6 showing significantly fewer features. (C) Bivariate heat map of feature depth versus area at pH 4. The red and yellow overlaid curves show tip-limited regions for r_{tip} = 8 and 4 nm, respectively, where a small-radius pore would read artificially shallow, as shown in the inset. Dashed black lines represent the top and bottom of the bilayer surface. Increasing probability density is shown in false color from purple to red. (D) Cartoons demonstrate how two equally deep pores spanning the entire thickness of the membrane, t, could result in two different depth measurements (here $r_{tip} = 2t = 8$ nm). (E) Distribution of effective radii of features constructed from analyzing >20 000 features at pH 4 (data, red line; fits, dashed lines). (Inset) Integrated radius distribution.

at the highest concentrations measured. In Figure 1D−F, we show the leakage as a function of pH for pHD15, pHD24, and pHD108. At the lowest concentrations, little or no leakage is observed at any pH. At the highest concentrations, leakage sharply transitions to 100% with decreasing pH. Under these conditions, the transition as a function of pH is steep, occurring over 1 pH unit. Such steepness likely indicates that the acidic residues protonate and deprotonate cooperatively.[18] Interestingly, we observe a large increase in pH50 as the peptide concentration is increased. Peptides pHD24 and pHD108 experience a shift of about 1 pH unit when the peptide concentration is increased from a P:L of 1:500 to 1:50. For pHD15, the shift is somewhat smaller at the P:L where it can be compared.

To further characterize the bilayer poration induced by the pHD peptides, we used atomic force microscopy (AFM). AFM can provide a direct visualization of peptide-induced topographical structure in supported lipid bilayers. Following recent studies on parent peptide MelP5 and the macrolittins,[19,20] we applied tapping mode AFM to image pHD108-induced membrane remodeling. Peptides and POPC vesicles were incubated prior to deposition onto freshly cleaved mica and then imaged in solution at an approximate P:L of 1:100. Data acquired at pH 4 exhibited numerous punctate porelike features (Figure 2A). Interestingly, when the pH of the imaging buffer was raised, the surface topography of the sample changed substantially. In particular, fewer punctate porelike features were observed at pH 6 (Figure 2B) than at pH 4. The average number of features was determined in 12 non-overlapping 500 × 500 nm^2 areas. The results indicate a 6-fold reduction in the average number of features from 248 (at pH 4) to 40 (at pH 6). If we restrain this analysis to features exhibiting effective radii smaller than 8 nm to exclude large voids or membrane defects, then there is an approximate order of magnitude reduction in the average number of punctate porelike features per area, from 215 (pH 4) to 20 (pH 6). A few large voids (or defects) in the bilayer were observed at both pH 4 and 6 and were relatively stable. Regardless of the metric, the change in pH had a marked effect on the peptide remodeling of the lipid bilayer. We note that it is unlikely that

DOI: 10.1021/jacs.9b01970
J. Am. Chem. Soc. 2019, 141, 6706−6718

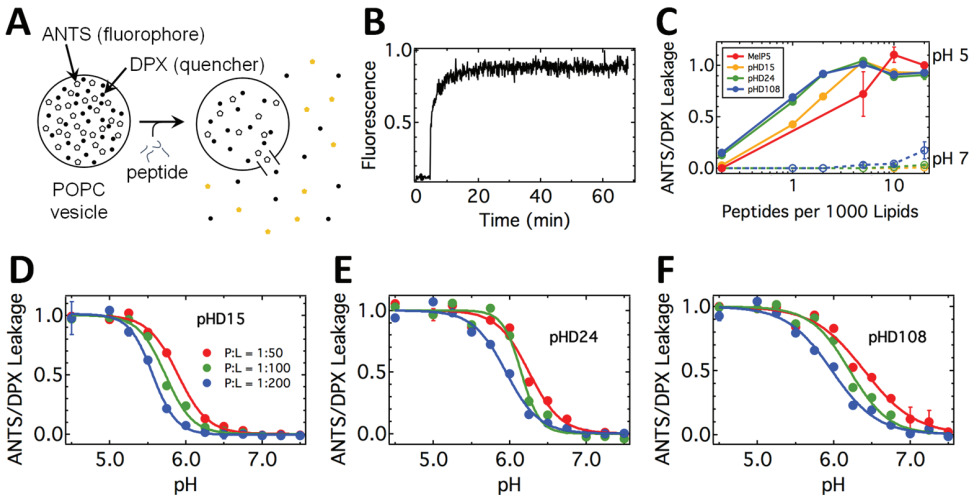

Figure 3. ANTS/DPX leakage assay. (A) Schematic of the assay. Peptides were incubated with POPC vesicles with encapsulated ANTS (fluorophore) and DPX (quencher) for 1 h. Upon pore formation, the dilution of ANTS and DPX results in an increase in ANTS fluorescence. (B) Time course of ANTS leakage by pHD108 at pH 5. ANTS fluorescence was monitored on a fluorimeter (ex/em = 350/519 nm). At about t = 3 min, peptide was added to a cuvette with 1 mM POPC vesicles for a final P:L of 1:100. After 1 h, Triton X100 was added to obtain the 100% leakage fluorescence value. (C) Leakage as a function of P:L. At pH 5, the pHD peptides are more potent than MelP5. At pH 7, (dashed lines) the peptides do not cause much leakage, even at the highest concentrations measured. (D–F) Leakage as a function of pH for pHD15 (D), pHD24 (E), and pHD108 (F).

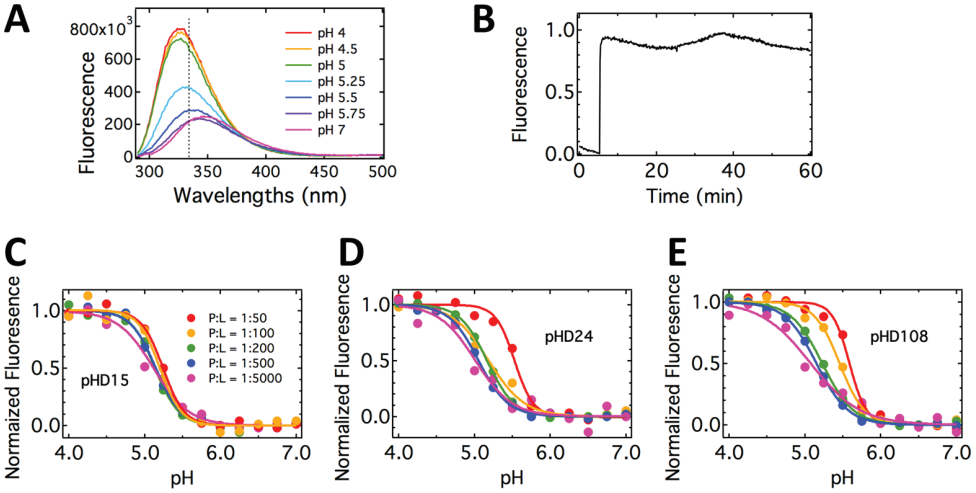

Figure 4. pHD peptide binding to lipid bilayers, as followed by tryptophan fluorescence. Each pHD peptide has one tryptophan, and its fluorescence is sensitive to the polarity of its environment. (A) Fluorescence spectra of pHD15 as a function of pH ranging from 4 to 7. Samples with 10 μM pHD15 and 1 mM POPC (P:L = 1:100) were incubated for 1 h before spectra were recorded. The dotted line is at 334 nm. (B) Time course of pHD108 tryptophan fluorescence. Upon addition of vesicles at about t = 5 min, binding is rapid. (C–E) Normalized fluorescence as a function of pH for pHD15 (C), pHD24 (D), and pHD108 (E).

the act of exchanging buffer itself would have such an effect on the lipid bilayer, as the bilayer sample was washed repeatedly (four times with 75 μL) with the pH 4 buffer prior to imaging. We note that in the absence of peptide the upper leaflet surface of a POPC bilayer is essentially featureless.[19]

To quantify pore like structures in a statistical manner, features were detected algorithmically from a series of AFM images at pH 4. Figure 2C shows a bivariate histogram of feature depths versus footprint area. Dashed black lines indicate the top and bottom of the bilayer, and overlaid red and yellow curves show tip-limited regions for two different assumed radii, r_{tip} = 8 and 4 nm, respectively. Features within this region have shallower depth readings, most likely as a result of the feature being too narrow for the tip to penetrate to the bottom, as shown by the cartoon inset. Features with larger areas tended to be deeper, approaching the expected 4 nm thickness of the membrane. Figure 2D demonstrates how two pores, both of which span the membrane, could result in two different depth measurements: one accurate and one artificially shallow. We also report the effective radius distribution of features at pH 4 (Figure 2E) as determined from Hessian blob analysis under the assumption of circularity (which matched many of the features). Three populations of radii were prominent: 3.2, 4.7, and 8.2 nm. Integration of the radius distribution (Figure 2E, inset) indicated that approximately 50% of the total features exhibited a radius ≥4.5 nm, consistent with the leakage of 40 kDa dextran (Stokes' radius ~4.5 nm). This analysis, coupled with the observation of fewer features

DOI: 10.1021/jacs.9b01970
J. Am. Chem. Soc. 2019, 141, 6706–6718

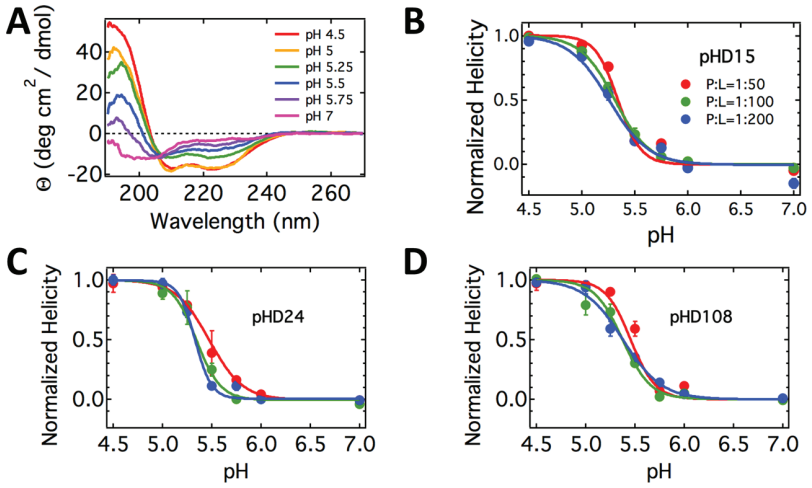

Figure 5. Secondary structure of the pHD peptides as a function of pH. (A) Circular dichroism spectra of pHD108 at P:L = 1:200, measured after 1 h of incubation with 1 mM POPC vesicles. Separate samples were made for each pH. (B–D) The % helicity, measured as a function of pH, was calculated from the absorbance at 222 nm and scaled from 0 and 1 for pHD15 (B), pHD24 (C), and pHD108 (D).

observed at higher pH, corroborates the aforementioned macromolecular poration studies and further suggests that many of the features identified via AFM are bona fide pores spanning the thickness of the membrane.

Small-Molecule Release in Response to the pHD Peptides. To determine if the pHD peptides form small pores at low peptide concentrations, we measured pore formation with an ANTS/DPX leakage assay, which detects the leakage of ~0.4 kDa ANTS.[21] Results from these assays are shown in Figure 3. Vesicles containing coencapsulated fluorophore (ANTS) and quencher (DPX) were incubated with peptide for 1 h. Figure 3A shows a schematic of the leakage assay. The crowding of ANTS and DPX within the vesicles quenches ANTS fluorescence. Pore formation results in ANTS/DPX release and a concomitant increase in ANTS fluorescence. In Figure 3B, we show the kinetics of leakage. Upon addition of peptide, ANTS fluorescence increases sharply and then reaches a plateau. The release of ANTS and DPX is rapid and very similar to TBD leakage, with greater than 90% leakage occurring over 10 min. In Figure 3C, we show the fractional leakage of ANTS and DPX, measured at 60 min, as a function of the peptide-to-lipid ratio. The peptides are very potent at pH 5, with substantial activity observed at concentrations of as low as P:L = 1:1000 and ≥95% activity at P:L = 1:200. Small-molecule release is more potent than macromolecule release (Figure 1). In small-molecule leakage, as with macromolecule leakage, pHD15 is less active than pHD24 and pHD108, and MelP5 is less active than pHD15, but the differences are smaller than for macromolecule release. Little or no ANTS leakage is observed at pH 7 for the pHD peptides, even at the highest concentrations measured. In Figure 3D–F, we show the leakage as a function of pH for pHD15, pHD24, and pHD108. At the concentrations shown, leakage sharply transitions to 100% with decreasing pH. The transition as a function of pH is steep. Again, pH50 increases as the peptide concentration is increased, with a shift of about 0.3 pH unit when the peptide concentration is increased from P:L = 1:200 to 1:50. For pHD24 and pHD108, pH50 increases from 6.0 to ~6.4. For pHD15, pH50 is lower; it increases from 5.6 to 5.9 as the peptide concentration is increased from 1:200 to 1:50.

Binding of the pHD Peptides to Membranes. We characterized the binding of the peptides as a function of pH and peptide concentration with tryptophan fluorescence titration.[13] As shown in Figure 4A, the fluorescence emission maximum shifts from ~350 nm at neutral pH to 330 nm at acidic pH, indicative of a transition from aqueous, exposed tryptophan to membrane-inserted tryptophan.[13] In Figure 4B, we show a kinetic trace of binding at pH 4.5 under conditions at which the peptide is active. Upon addition of peptide to a 1 mM vesicle solution at t = 8 min, binding occurs rapidly and is essentially complete in 1 min. In Figure 4C–E, we show the scaled fluorescence intensities at 335 nm as a function of pH for different peptide concentrations for pHD15, pHD24, and pHD108. In all cases, binding is dependent on pH, with a sharp transition occurring over about 1 pH unit, which is indicative of cooperativity. Peptides pHD108 and pHD24 show a small increase in pH50 and a sharper slope as the peptide concentration is increased. pH50 increases from 5.1 to 5.6 for pHD108 and from 5.0 to 5.5 for pHD24 as P:L increases from 1:5000 to 1:50.

Acquisition of Secondary Structure upon Membrane Binding. To determine the secondary structure of the peptides, we used circular dichroism (CD) spectroscopy. We could study peptides only at the three highest peptide concentrations because the technique lacks high sensitivity. As shown in Figure 5A, the CD spectra of the pHD peptides transition from a spectrum typical of a random coil with one minimum at 200 nm at pH 7 to a spectrum characteristic of an α-helix with two minima at 208 and 220 nm at pH 4.5. The spectra indicate that the pHD peptides undergo transitions from random coil to α-helix as the pH is decreased from 7 to 4.5. In Figure 5B–D, we show the relative % helicity as a function of pH and P:L for pHD15, pHD24, and pHD108. Folding, like binding and leakage, is dependent on pH and exhibits a cooperative transition occurring over 1 pH unit. All peptides show little to no change in pH50 as the peptide concentration is increased over the available range. pH50 for pHD15 is 5.3 ± 0.1 for all P:L. For pHD24, pH50 increases from 5.3 to 5.5, and for pHD108, pH50 increases from 5.4 to 5.5 as P:L increases from 1:200 to 1:50. .

DOI: 10.1021/jacs.9b01970
J. Am. Chem. Soc. 2019, 141, 6706–6718

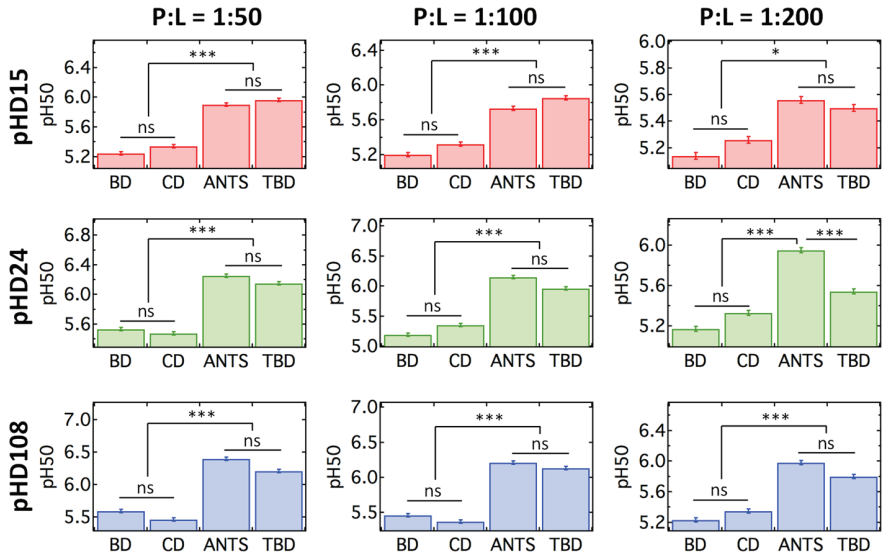

Figure 6. Comparison of pH50s for binding (BD), folding (CD), ANTS/DPX leakage (ANTS), and TAMRA-biotin-dextran leakage (TBD) pK_a's. Significance was calculated by ANOVA and a Tukey test for multiple comparisons, where **** indicates $P < 0.0001$, *** indicates $P = 0.0001$ to 0.001, ** indicates $P = 0.001$ to 0.01, * indicates $P = 0.01$ to 0.05, and ns indicates $P \geq 0.05$.

Comparison of pH50 Values for the Binding, Folding, and Leakage of Vesicle Contents. In Figure 6, we compare the pH dependence of binding, folding, small-molecule leakage, and macromolecular leakage for the three highest peptide concentrations for pHD15, pHD24, and pHD108. Several features are common for all peptides at all P:L ratios. First, the differences in pH50 values for binding and helicity are not statistically significant, which is expected given the binding−folding coupling that is typical of membrane-active peptides.[22] pH50 for binding and structure also do not depend strongly on peptide concentration (discussed below). Second, the differences in pH50 for dextran and ANTS/DPX leakage are not statistically significant, with one exception. Third, and most interesting, the pH50 values for binding and helicity are always significantly lower than the pH50 for leakage. This effect is most pronounced at high peptide concentrations, a consequence of the observation in Figures 1 and 3 that the pH50 values for leakage increase with increasing peptide concentration.

Comparison of Binding and Dextran Leakage pH50s. An intriguing consequence of the higher pH50 of leakage compared to that of binding and folding is that at a high overall peptide-to-lipid ratio, leakage is high despite the fact that binding and helicity appear to be negligible. In Figure 7, we compare the binding and dextran leakage curves for pHD15, pHD24, and pHD108 as a function of pH and the peptide-to-lipid ratio. At P:L = 1:50 (top row), the binding and leakage curves are offset such that pH50 for binding is lower than that for leakage. At high P:L, the greatest discrepancies in the fraction bound and the fraction leakage occur at intermediate pH values. For example, at pH 5.75, pHD15 induces 96% TBD leakage when only 3% of the peptide is bound. At low P:L, the converse is true: leakage is close to zero despite the fact that the fraction bound is high. At P:L = 1:5000, the pH50 for binding for pHD15 is 5.12 ± 0.05. The pH50 for leakage cannot be calculated because no leakage is observed at any pH. The large discrepancies between fraction bound and fraction leakage indicate that the fractional leakage is not dependent on the fraction of peptide bound or folded.

Leakage Is Dependent on the Number of Peptides Bound per Vesicle. We sought to explain the discrepancies between fractional leakage and fraction bound by accounting for the actual amount of peptide that is bound to membranes under the different conditions. Because only bound peptides can induce pore formation, we calculated the number of peptides that are bound per lipid, under each condition, to determine if leakage scales with this variable. In Figure 8A, we show leakage as a function of bound peptide per lipid for pHD15 (red), pHD24 (green), and pHD108 (blue). Plotted in this way, all of the data for all three pHD peptides can be fitted by a single curve (solid black line), indicating that the pHD peptide function depends solely on the amount of bound peptide. Leakage of 50% occurs when 1 peptide is bound per 1300 lipids, a manifestation of the exquisite potency of the pHD peptides because we know of no other peptide, except the closely related macrolittins,[20] that approach this potency for macromolecular poration.

Assuming an area per lipid of 70 Å^2,[23] it can be estimated that there are about ~90 000 lipids per vesicle.[24] In Figure 8B, we rescale the data in Figure 8A, now plotting the leakage as a function of bound peptides per vesicle. The different colors in Figure 8B indicate the different pH values and provide an illustration of the fact that the pH controls function entirely by controlling the amount of bound peptide. In Figure 8B, we further see that 50% leakage occurs when only 75 peptides are bound per vesicle.

To rationalize these data, in Figure 8C we plot the Poisson distribution of peptides per vesicle, when averages are 10, 75, and 250 peptides per vesicle, corresponding to the cases of no leakage, 50% leakage, and 100% leakage (according to Figure 8B). We further estimate the number of peptides required to line a pore that permits the passage of a 40 kDa dextran through the bilayer. In particular, we reason that the pore must have a radius that is at least equal to the hydrodynamic radius of 40 kDa dextran: 4.5 nm. If we assume that the peptides are in contact with each other and that the diameter of the pHD helix, with side chains included, is 1.2 nm, then we calculate that 20−30 peptides are required to line the perimeter of such

DOI: 10.1021/jacs.9b01970
J. Am. Chem. Soc. 2019, 141, 6706−6718

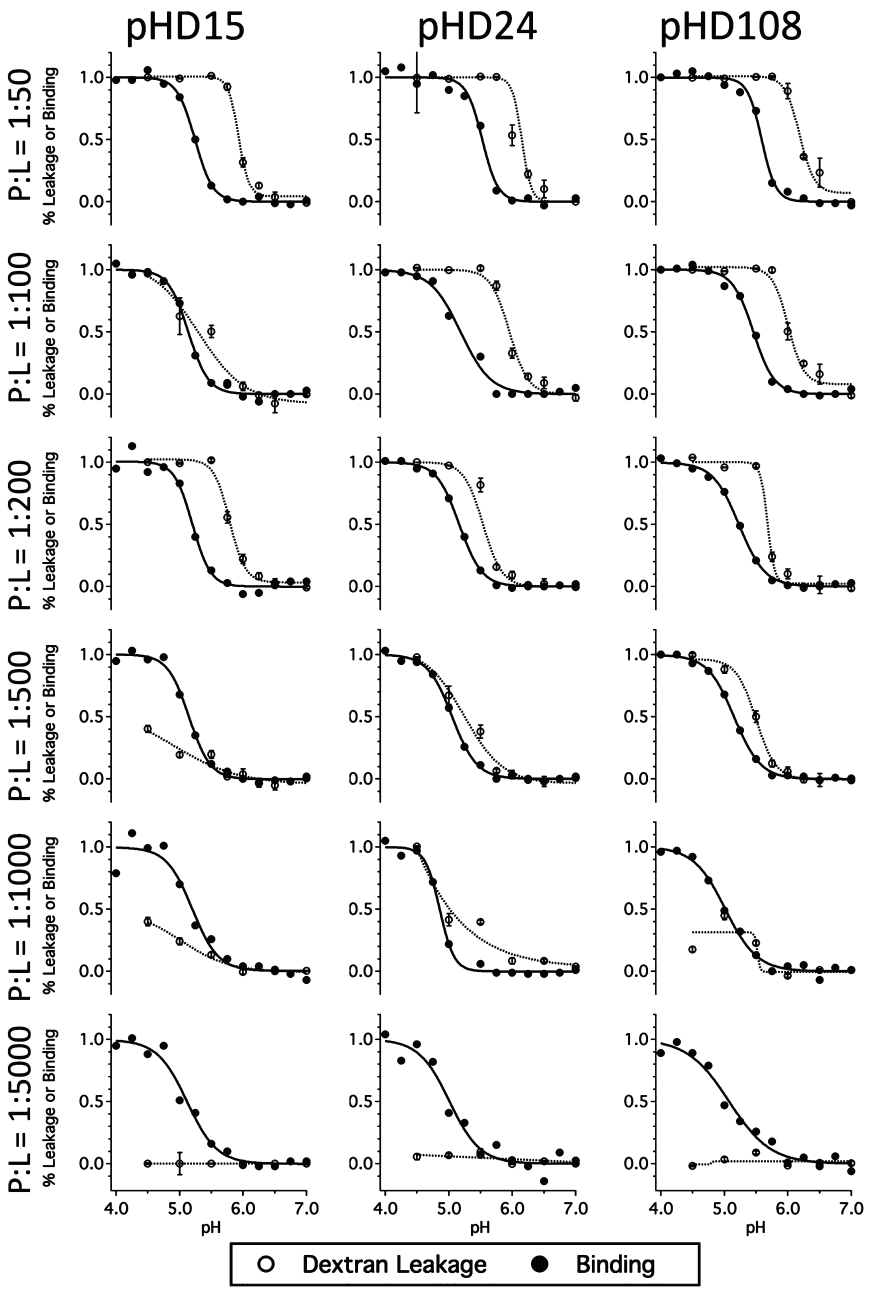

Figure 7. Comparison of binding and dextran leakage activity curves as a function of pH and P:L. At the highest P:L, 100% leakage is possible when only a small fraction of peptide is bound, and at the lowest P:L, no leakage occurs even when all peptide is bound.

a pore. This is called a barrel-stave pore.[25] Thus, little macromolecule leakage can be expected when fewer than 20 peptides are bound per vesicle, consistent with the experiment. At least partial leakage becomes possible once the 20−30 peptide cutoff is exceeded. It is also possible that the peptides form toroidal pores, lined by both peptides and lipid headgroups.[25] In this case, fewer peptides would be required to line the pore. On the other hand, some peptides could line nonproductive pores with diameters that are too small to allow the passage the 40 kDa dextran. Indeed, the AFM data in Figure 2A,E show that the most probable pore radius is about 3 nm and is thus too small for dextran passage. Overall, the partial leakage that is observed experimentally at <100 peptides per vesicle is consistent with most of the vesicle-bound peptides participating in one or a few pores.

Dynamics of Peptide Association with Membranes. Because a small fraction of bound peptides can cause substantial leakage, it is possible that the pHD peptides can exchange between vesicles and induce pores on multiple vesicles while the overall fraction of bound peptide remains low. We tested this possibility by evaluating if membrane-bound pHD15 can transfer to new vesicles composed of the brominated lipid, diBrPSPC. The bromines, located on the 9,10 positions on the acyl chains of the lipids, will quench tryptophan when the peptide is bound to membranes[14] (Figure 9A). Therefore, exchange from POPC to diBrPSPC will lead to quenching. To test for this possibility, pHD15 was

DOI: 10.1021/jacs.9b01970
J. Am. Chem. Soc. 2019, 141, 6706−6718

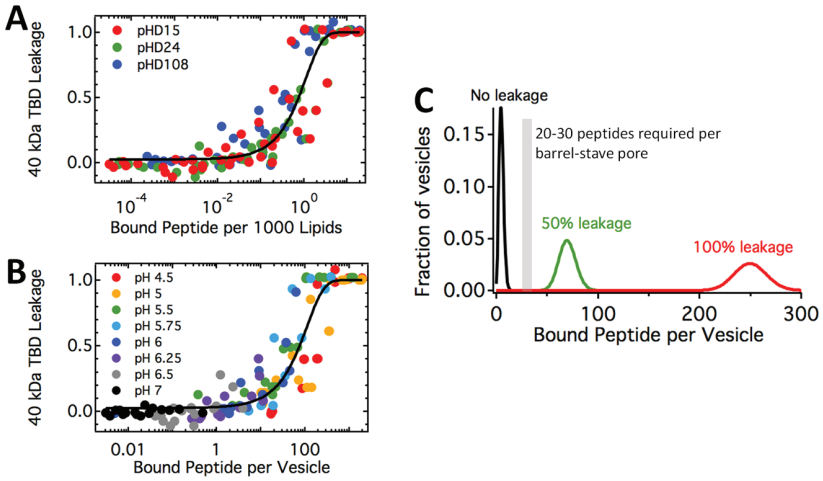

Figure 8. Activity of the pHD peptides depends on the number of bound peptides per vesicle. (A) Dextran leakage as a function of bound peptide per lipid for the three peptides: red, pHD15; green, pHD24; and blue, pHD108. Leakage (50%) occurs when roughly 1 peptide is bound per 1300 lipids. (B) The same as in panel A but replotted as a function of bound peptides per vesicle, assuming that each vesicle has ~90 000 lipids. The different colors indicate the different pH values used in the experiment. Leakage (50%) occurs when on average 75 peptides are bound per vesicle. (C) Poisson distribution of peptides per vesicle, when averages are 10, 75, and 250 peptides per vesicle. The data in panel B show that in these three cases we observe no leakage, 50% leakage, and 100% leakage, respectively. This result can be rationalized, as we calculate that 20−30 peptides are needed to form a barrel-stave pore of ~4.5 nm diameter to allow for the passage of 40 kDa dextran. Thus, no leakage is expected when fewer than 20 peptides are bound per vesicle. Only partial leakage is expected when ~75 peptides are bound, as the pore size distribution in Figure 2 favors pores that are smaller than 5 nm in diameter. Leakage (100%) is expected when more than 200 peptides are bound per vesicle.

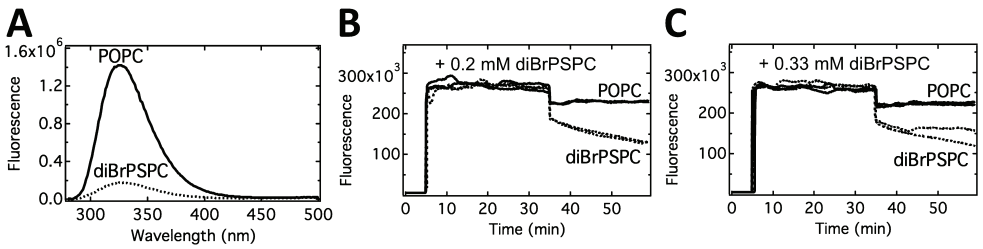

Figure 9. Quenching of tryptophan fluorescence by the redistribution of pHD peptides. (A) pHD15 bound to vesicles composed of diBrPSPC displays quenched fluorescence. Peptide at 20 μM was incubated with 1 mM vesicles at pH 4.5 for 1 h before the emission spectra of tryptophan was measured (ex = 270, em = 280−500 nm). Peptides in the presence of vesicles composed of POPC or diBrPSPC show blue-shifted fluorescence, indicating that the peptide is bound. However, the tryptophan peak, in the presence of brominated lipids, is 87% lower in intensity. (B) Tryptophan fluorescence as a function of time upon the addition of a second batch of vesicles. Original samples are prepared with 1 mM vesicles. At t = 500 s, 20 μM pHD15 is added. After about 30 min, 0.2 mM POPC or diBrPSPC vesicles are added to the cuvette. (C) Same time course as in panel B, but 0.33 mM new vesicles are added after 30 min.

incubated with 1 mM POPC vesicles at pH 4.5, where ≥95% of the peptides are bound (Figure 4C). After 0.2 mM POPC or diBrPSPC vesicles were added, the tryptophan fluorescence intensity decreased (Figure 9B). The decrease caused by PC vesicles can be explained by dilution; however, the rapid and much larger decrease into diBrPSPC vesicles suggests that peptides, initially bound to POPC vesicles, are rapidly quenched by diBRPC lipids with a half-time of a few seconds. Quenching is greater when more diBrPSPC is added (Figure 9C). Most likely, the observed quenching is due to the rapid transfer of peptides between vesicles. However, it is also possible that the peptides mediate the fusion of diBrPC and POPC vesicles.

Dynamics of Pore Formation. Pore dynamics, if present, can be revealed by repeatedly scanning the AFM tip over the "same" membrane area. Figure 10A−C provides an example. The three images shown were acquired at 3 min intervals (i.e., t = 0, 180, and 360 s). Two general classes of porelike features can be identified: those which are stable on the time scale of minutes (red arrows) and those which are metastable (i.e., can be visualized only in a single image frame (white circles and white arrows) and then essentially disappear). For example, the white dashed circle indicates the absence (Figure 10A), presence (Figure 10B), and subsequent absence (Figure 10C) of a porelike feature at approximately the same location on the membrane surface, as verified by the large stable void in the center right of all images which serves as a reference. In addition, the white arrow indicates a porelike feature in Figure 10A which is absent in the other image frames.

To provide a more detailed view of pore dynamics, we acquired kymograph data (Figure 10D−F). Here, the slow axis of the AFM raster scan was disabled, allowing the tip to scan back and forth laterally over (approximately) the same portion of the membrane surface. The resulting time versus position plots reinforce the bimodal behavior identified in the regular images. A kymograph of a relatively static porelike feature is shown in Figure 10D. Over this ~18 s time course, the topographic distortion of the membrane induced by the

DOI: 10.1021/jacs.9b01970
J. Am. Chem. Soc. 2019, 141, 6706−6718

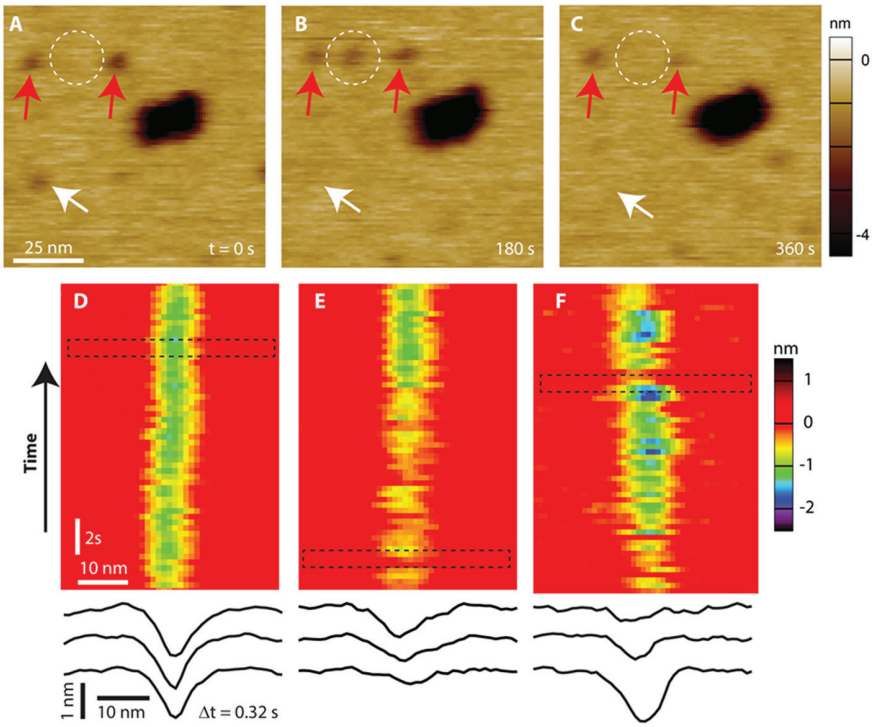

Figure 10. Dynamics of pHD108-induced bilayer topography. (A–C) Time-lapse images of a membrane area. White arrows and circles highlight features which appear or disappear on the time scale of image acquisition, and red arrows highlight relatively static features. The time interval between images was 180 s. (D–F) Kymographs (time versus position) of porelike features that were stable (D) or displayed significant temporal dynamics, as evidenced by rapid changes in depth and area (E and F). Sets of three sequential line scans are displayed below each kymograph (from the dashed rectangular boxes). The time interval between individual line scans within each set was 0.32 s. All data shown here were acquired at pH 4.

peptide was relatively stable, measuring about 1 nm deep over the entire trace. In contrast, the other two kymographs (Figure 10E,F) display rich and varied dynamics characterized by significant saltatory changes on subsecond time scales. Differences in conformation and conformational dynamics are also evident in the triplets of line scans shown below each kymograph. Line scans within a set (located by the black dashed rectangles superimposed on the kymographs) are separated temporally by 0.32 s. Clearly, the line scans shown in Figure 10D are indicative of a more stable topographic structure than those in Figure 10E,F. Further work will be required to quantify the relative populations of stable versus metastable features from the AFM data.

DISCUSSION

Here we have studied membrane interactions, secondary structure, and the function of the pHD peptides across a range of peptide concentrations and pH values to better understand their sequence–structure–function relationships. Overall, the observed dependencies of binding, structure, and membrane permeabilization on pH are sigmoidal with sharp transitions that occur, in most cases, over ~1 pH unit. In comparison, an unaltered protonation equilibrium will be much shallower (e.g., protonation as described by the Henderson–Hasselbalch equation occurs over about 2.6 pH units, for a 5 to 95% transition). This suggests that the protonation/deprotonation of the acidic residues occurs synergistically. The free energy of membrane binding likely contributes to the observed cooperativity. The pH50 values, ranging from 5.0 to 6.4 for the various measurements reported here, are significantly higher than the inherent pK_a values of isolated Asp and Glu side chains, (~3.5), further implying that there are significant interactions between these side chains and that they are not acting independently. Indeed, the charges engineered into the pHD library are positioned with helical spacings so that they will repel one another maximally when the peptide has α-helical structure. The very fact that the screen selected only for peptides with five or six acidic residues suggests that the synergistic interactions between the charges is critical for pHD function.

Cooperativity in Binding. For peptide binding, positive cooperativity with peptide concentration will arise if there are strong attractive interactions between peptides in the membranes that are at least as energetic as the peptide–membrane interactions. This can occur if peptides self-assemble tightly into higher-order oligomeric structures in the membrane. While this effect has been reported at least once,[26] it is not frequently observed probably because membrane partitioning is inherently stronger than the likely magnitude of peptide–peptide interactions in membranes. Alternately, if the presence of peptides in the membrane changes the membrane structure in a way that improves the binding of additional peptides, then positive cooperativity could be observed. This scenario could occur, for example, if the expansion of a membrane pore is more energetically favorable (or less costly) than its initial formation of the pore.

For the pHD peptides, positive cooperativity will result in a rightward shift of the pH binding curves for higher total peptide concentration. With pHD24 and pHD108, we indeed observed small upward shifts in pH50 for binding at the

DOI: 10.1021/jacs.9b01970
J. Am. Chem. Soc. 2019, 141, 6706–6718

highest peptide concentrations, suggesting positive cooperativity (Figure 4). However, given that the peptide concentrations varied by 100-fold, the cooperativity is small. The binding of one peptide to the bilayer is not strongly influenced by the presence of other peptides already bound to the membrane. Peptide−membrane interactions are dominant over peptide−peptide interactions. Thus, we can describe pHD peptide binding and folding in classical thermodynamic terms of membrane partitioning.[24,27,28]

Coupling of Binding and Folding. The actions of peptides that bind to membranes are usually considered within the framework of a canonical thermodynamic model that includes coupled partitioning of the peptide into the membrane and the acquisition of secondary structure.[27,29] This well-supported concept of binding−folding coupling is a consequence of the high energetic penalty of partitioning open peptide bonds into the membrane, relative to a peptide bond that is involved in hydrogen-bonded secondary structure.[29] For the pHD peptides, the observable properties are intentionally coupled to the protonation states of the five or six acidic residues that were identified in the high-throughput screen.[11] Potential acidic residues in the library were placed with helical spacing patterns to maximize their influence on binding and structure propensity. Here, we show that binding and folding have very similar dependencies on peptide concentrations and pH, at least for the conditions under which both could be measured. We observe a small positive cooperativity in binding that is not apparent in secondary structure measurements, but the latter is a less-sensitive measurement overall and can be measured for only the highest few peptide concentrations. In any event, the pH50 values for binding and folding are not significantly different from one another (Figure 6). They are coupled; binding does not occur without folding and folding does not occur without binding. The steepness of the pH curves and the upward shift in pH50 compared to free carboxylate groups shows that there is also coupling of protonation to binding and secondary structure. The fully deprotonated peptides do not interact with membranes or fold into α-helices, while the protonation of at least some acidic side chains enables membrane interaction and folding.

pH Dependence and Concentration Dependence of Permeabilization. We also measured the dependence of *function*, membrane permeabilization to macromolecules, on pH and peptide concentration. The behavior of function is very different from that of binding and structure. In this case, the pH50 values and slopes vary significantly with the total peptide concentration. At the highest peptide concentrations, the pH50 values for leakage are the highest, and the pH curves are the steepest. As the peptide concentration is decreased, pH50 and the slope both decrease. However, slopes, when measurable, are never as shallow as predicted for simple protonation equilibrium, and pH50 values are never as low as expected for a water-exposed carboxyl side chain.

For comparison, we also measured the pH50 values for the leakage of small-molecule ANTS at several peptide concentrations. The pH50 values for ANTS leakage and for dextran leakage are statistically indistinguishable from one another. This demonstrates that pore formation for small molecules and pore formation for macromolecules are not distinct processes. Small-molecule leakage occurs at lower P_{bound}/L because there is a distribution of pore sizes (Figure 2), only some of which can pass macromolecules, but smaller and larger pores form with the same pH50.

Coupling of Binding and Poration. Interestingly, the functional data show that efficient poration can occur at pH values significantly higher than those that enable efficient binding, an effect that becomes greater for higher peptide concentrations (Figure 7). Indeed, there are pH values at which substantial macromolecule leakage occurs despite the fact that fractional binding and folding are very small. There are also conditions where there is no leakage despite 100% binding (Figure 7, bottom row). It might seem paradoxical that binding/folding are not tightly coupled to function (poration). However, this paradox is resolved when we consider the dependence of vesicle permeabilization on the peptide *bound* per lipid rather than total peptide per lipid (Figure 8). When the functional data are plotted as a function of P_{bound}/L (i.e., the actual concentration of peptide acting on the membranes), the curves, slopes, and pH50 values for the various concentrations become similar for all three peptides under all conditions. Leakage depends primarily on how many peptides are bound per vesicle, and thus binding and poration are in fact tightly correlated. The apparent paradox occurs because small *fractional* binding can drive efficient permeabilization under conditions in which P_{total}/L is much higher than the P_{bound}/L required for permeabilization.

It is interesting that the poration curves as functions of P_{bound}/L behave as a single function despite data that was collected between pH 4.5 and pH 6.5. We conclude from this observation that the structure of the pore is not sensitive to pH in this range. As long as the protonation state enables some pHD peptide to bind, the pore can be formed.

Potency: Number of Peptides Required to Permeabilize a Vesicle. The plot of macromolecule leakage versus P_{bound}/L in Figure 8A shows that the concentration that drives 50% permeabilization of PC vesicles to 40 kDa dextran is around P_{bound}/L = 1:1300 under all conditions. This is equivalent to 75 peptides per vesicle. The only other membrane-permeabilizing peptides known that have this degree of potency for releasing macromolecules from PC vesicles are the closely related macrolittins,[20] which were selected from the same library.

Assuming a random dispersal of peptides, a Poisson function will describe the distributions of the number of peptides per vesicle (Figure 8C). On the basis of the calculation that 20−30 peptides are needed to form a barrel-stave pore of ∼4.5 nm diameter to allow for the passage of 40 kDa dextran (4.5 nm hydrodynamic radius), we can expect no leakage when fewer than 20 peptides are bound per vesicle, and indeed we observe no leakage in this case. Only partial leakage can be expected when 75 peptides are bound, as the pore size distribution shown in Figure 2 favors pores that are smaller than the hydrodynamic radius of the dextran probe. Consistent with this expectation, experimentally we observe 50% leakage when 75 peptides are bound per vesicle (Figure 8B). We observe 100% leakage once about 200 peptides are bound to each vesicle.

Possible Pore Structure. Taken together, the highly potent macromolecular leakage and the large pores observed by AFM suggest a structural hypothesis for the pHD peptides. At low pH, when at least some of the acidic groups are protonated, the pHD peptides bind to membranes and fold into amphipathic α-helices. We hypothesize that these amphipathic helices stabilize exposed bilayer edges, enabling the otherwise energetically unfavorable formation of large open pores. We envision that the amphipathic helices lie at the bilayer edge, exposing charged and polar groups to the aqueous

DOI: 10.1021/jacs.9b01970
J. Am. Chem. Soc. 2019, 141, 6706−6718

phase while exposing the hydrophobic surfaces of the helices to the bilayer. Perhaps the pore edges are further stabilized by lateral electrostatic interactions between acidic side chains and the two basic residues on the pHD peptides.

Our recent description of the macrolittins,[20] closely related peptides that also have very potent macromolecular poration activity at pH 7, supports these conclusions. The macrolittins were selected from the same library as the pHD peptides except that they were selected for their ability to permeabilize bilayers to macromolecules at pH 7. They are nearly identical to the pHD peptides in sequence, structure, and potency except that they have three acidic residues total compared to five or six in the pHD peptides. In the pHD peptides, the protonation of several residues in the other acidic positions enables the pore structure to form only at acidic pH, while in the macrolittins this pore structure is possible at pH 7 because of the smaller number of acidic residues.

By oriented circular dichroism, the parent peptide of the pHD library, MelP5, resides in a mostly membrane-spanning, perpendicular orientation.[30] The same is true for the macrolittins.[20] Thus, it is likely that the pHD peptides are also mostly perpendicular to the membrane plane at acidic pH. However, it is difficult to study the orientation of the pHD peptides because it is difficult to control or determine the effective pH in the typical oriented CD sample, a stacked multibilayer system that is hydrated through the vapor phase.[31−33] Furthermore, AFM has shown that MelP5 causes membrane thinning in the vicinity of the pores, while the macrolittins and pHD peptides cause pores but not much membrane thinning.[19,20] Thus, by progressing from MelP5 to the pHD peptides and macrolittins, we have evolved peptides that more effectively span the bilayer "edge" and enable large pores to form in the membrane. AFM shows the dynamic nature of the pores as they come in and out of existence on the time scale of seconds to minutes (Figure 10).

Effect of Sequence. The physical chemistry and sequence of the pHD peptides affect their potency and pH dependence. For instance, pHD15 has a lower potency and a lower pH50 compared to those of the other two peptides (Figure 1), suggesting a sequence-dependent effect that may be due to the number of acidic residues; pHD15 is the only pHD peptide with six acidic residues instead of the usual five. On the other hand, the most potent peptide, pHD108, has five glutamic acids, which were significantly overrepresented in the pHD sequences, whereas pHD15 and pHD24 have three and two aspartic acids, respectively. These observations of sequence-specific effects suggest that additional changes in sequence, which can be either rationally engineered or identified via high-throughput screens from peptide libraries, can be used to fine tune the properties of the pHD peptides for desired applications.

CONCLUSIONS

Here we study the mechanism of action of the pHD peptides, which form large pores in POPC bilayers in a pH-dependent manner. The activity of these highly potent peptides is controlled by both pH and peptide concentration and ultimately depends on the number of peptides that are bound per vesicle. The physical−chemical sequence−structure−function relationships that we described here will be useful in the future design and optimization of membrane permeabilizing peptides for specific applications. Such applications could include the release of endosomal contents for drug delivery upon acidification as well as anticancer therapies that exploit the low pH of the tumor environment.

AUTHOR INFORMATION

Corresponding Authors

*kh@jhu.edu.
*kinggm@missouri.edu.
*wwimley@tulane.edu.

ORCID

Sarah Y. Kim: 0000-0003-1500-4955
Elmer Zapata-Mercado: 0000-0002-9766-8124
Gavin M. King: 0000-0002-5811-7012
William C. Wimley: 0000-0003-2967-5186
Kalina Hristova: 0000-0003-4274-4406

Notes

The authors declare no competing financial interest.

ACKNOWLEDGMENTS

Funded by NSF DMR 1709892 (K.H.), NSF DMR 1709792 (G.M.K.) and NIH R01 GM111824 and NSF DMR 1710053 (W.C.W.).

REFERENCES

(1) Nishimura, Y.; Takeda, K.; Ezawa, R.; Ishii, J.; Ogino, C.; Kondo, A. A display of pH-sensitive fusogenic GALA peptide facilitates endosomal escape from a Bio-nanocapsule via an endocytic uptake pathway. *J. Nanobiotechnol.* **2014**, *12*, 11.

(2) Bechinger, B. Towards membrane protein design: pH-sensitive topology of histidine-containing polypeptides. *J. Mol. Biol.* **1996**, *263*, 768−775.

(3) Moulay, G.; Leborgne, C.; Mason, A. J.; Aisenbrey, C.; Kichler, A.; Bechinger, B. Histidine-rich designer peptides of the LAH4 family promote cell delivery of a multitude of cargo. *J. Pept. Sci.* **2017**, *23*, 320−328.

(4) Yao, L.; Daniels, J.; Wijesinghe, D.; Andreev, O. A.; Reshetnyak, Y. K. pHLIP (R)-mediated delivery of PEGylated liposomes to cancer cells. *J. Controlled Release* **2013**, *167*, 228−237.

(5) Andreev, O. A.; Engelman, D. M.; Reshetnyak, Y. K. pH-sensitive membrane peptides (pHLIPs) as a novel class of delivery agents. *Mol. Membr. Biol.* **2010**, *27*, 341−352.

(6) An, M.; Wijesinghe, D.; Andreev, O. A.; Reshetnyak, Y. K.; Engelman, D. M. pH-(low)-insertion-peptide (pHLIP) translocation of membrane impermeable phalloidin toxin inhibits cancer cell proliferation. *Proc. Natl. Acad. Sci. U. S. A.* **2010**, *107*, 20246−20250.

(7) Parente, R. A.; Nir, S.; Szoka, F. C., Jr. Mechanism of leakage of phospholipid vesicle contents induced by the peptide GALA. *Biochemistry* **1990**, *29*, 8720−8728.

(8) Fendos, J.; Barrera, F. N.; Engelman, D. M. Aspartate Embedding Depth Affects pHLIP's Insertion pK(a). *Biochemistry* **2013**, *52*, 4595−4604.

(9) Wiedman, G.; Fuselier, T.; He, J.; Searson, P. C.; Hristova, K.; Wimley, W. C. Highly Efficient Macromolecule-Sized Poration of Lipid Bilayers by a Synthetically Evolved Peptide. *J. Am. Chem. Soc.* **2014**, *136*, 4724−4731.

(10) Wiedman, G.; Wimley, W. C.; Hristova, K. Testing the limits of rational design by engineering pH sensitivity into membrane-active peptides. *Biochim. Biophys. Acta, Biomembr.* **2015**, *1848*, 951−957.

(11) Wiedman, G.; Kim, S. Y.; Zapata-Mercado, E.; Wimley, W. C.; Hristova, K. pH-Triggered, Macromolecule-Sized Poration of Lipid Bilayers by Synthetically Evolved Peptides. *J. Am. Chem. Soc.* **2017**, *139*, 937−945.

(12) Stewart, J. C. Colorimetric determination of phospholipids with ammonium ferrothiocyanate. *Anal. Biochem.* **1980**, *104*, 10−14.

DOI: 10.1021/jacs.9b01970
J. Am. Chem. Soc. 2019, 141, 6706−6718

(13) Ladokhin, A. S.; Jayasinghe, S.; White, S. H. How to measure and analyze tryptophan fluorescence in membranes properly, and why bother? *Anal. Biochem.* **2000**, *285*, 235−245.
(14) Ladokhin, A. S. Distribution analysis of depth-dependent fluorescence quenching in membranes: A practical guide. *Methods Enzymol.* **1997**, *278*, 462−473.
(15) Mingeot-Leclercq, M. P.; Deleu, M.; Brasseur, R.; Dufrene, Y. F. Atomic force microscopy of supported lipid bilayers. *Nat. Protoc.* **2008**, *3*, 1654−1659.
(16) Marsh, B. P.; Chada, N.; Sanganna Gari, R. R.; Sigdel, K. P.; King, G. M. The Hessian Blob Algorithm: Precise Particle Detection in Atomic Force Microscopy Imagery. *Sci. Rep.* **2018**, *8*, 978.
(17) Bohrer, M. P.; Deen, W. M.; Robertson, C. R.; Troy, J. L.; Brenner, B. M. Influence of molecular configuration on the passage of macromolecules across glomerular capillary wall. *J. Gen. Physiol.* **1979**, *74*, 583−593.
(18) Hunt, J. F.; Rath, P.; Rothschild, K. J.; Engelman, D. M. Spontaneous, pH-dependent membrane insertion of a transbilayer à-helix. *Biochemistry* **1997**, *36*, 15177−15192.
(19) Pittman, A. E.; Marsh, B. P.; King, G. M. Conformations and Dynamic Transitions of a Melittin Derivative That Forms Macromolecule-Sized Pores in Lipid Bilayers. *Langmuir* **2018**, *34*, 8393−8399.
(20) Li, S.; Kim, S. Y.; Pittman, A. E.; King, G. M.; Wimley, W. C.; Hristova, K. Potent Macromolecule-Sized Poration of Lipid Bilayers by the Macrolittins, A Synthetically Evolved Family of Pore-Forming Peptides. *J. Am. Chem. Soc.* **2018**, *140*, 6441−6447.
(21) Ladokhin, A. S.; Wimley, W. C.; Hristova, K.; White, S. H. Mechanism of leakage of contents of membrane vesicles determined by fluorescence requenching. *Methods Enzymol.* **1997**, *278*, 474−486.
(22) Kaiser, E. T.; Kzdy, F. J. Secondary structures of proteins and peptides in amphiphilic environments (A review). *Proc. Natl. Acad. Sci. U. S. A.* **1983**, *80*, 1137−1143.
(23) Cornell, B. A.; Separovic, F. Membrane thickness and acyl chain length. *Biochim. Biophys. Acta, Biomembr.* **1983**, *733*, 189−193.
(24) Wimley, W. C. Describing the mechanism of antimicrobial peptide action with the interfacial activity model. *ACS Chem. Biol.* **2010**, *5*, 905−917.
(25) Sani, M. A.; Separovic, F. How Membrane-Active Peptides Get into Lipid Membranes. *Acc. Chem. Res.* **2016**, *49*, 1130−1138.
(26) Wimley, W. C.; Hristova, K.; Ladokhin, A. S.; Silvestro, L.; Axelsen, P. H.; White, S. H. Folding of á-sheet membrane proteins: A hydrophobic hexapeptide model. *J. Mol. Biol.* **1998**, *277*, 1091−1110.
(27) White, S. H.; Wimley, W. C. Membrane protein folding and stability: Physical principles. *Annu. Rev. Biophys. Biomol. Struct.* **1999**, *28*, 319−365.
(28) White, S. H.; Wimley, W. C.; Ladokhin, A. S.; Hristova, K. Protein folding in membranes: Determining the energetics of peptide-bilayer interactions. *Methods Enzymol.* **1998**, *295*, 62−87.
(29) Wimley, W. C.; White, S. H. Experimentally determined hydrophobicity scale for proteins at membrane interfaces. *Nat. Struct. Mol. Biol.* **1996**, *3*, 842−848.
(30) Krauson, A. J.; He, J.; Wimley, W. C. Gain-of-Function Analogues of the Pore-Forming Peptide Melittin Selected by Orthogonal High-Throughput Screening. *J. Am. Chem. Soc.* **2012**, *134*, 12732−12741.
(31) Wu, Y.; Huang, H. W.; Olah, G. A. Method of oriented circular dichroism. *Biophys. J.* **1990**, *57*, 797−806.
(32) Hristova, K.; Wimley, W. C.; Mishra, V. K.; Anantharamaiah, G. M.; Segrest, J. P.; White, S. H. An amphipathic à-helix at a membrane interface: A structural study using a novel x-ray diffraction method. *J. Mol. Biol.* **1999**, *290*, 99−117.
(33) Hristova, K.; Dempsey, C. E.; White, S. H. Structure, location, and lipid perturbations of melittin at the membrane interface. *Biophys. J.* **2001**, *80*, 801−811.

DOI: 10.1021/jacs.9b01970
J. Am. Chem. Soc. 2019, 141, 6706−6718